

PAPER

## Low thermal conductivity of peanut-shaped carbon nanotube and its insensitive response to uniaxial strain

To cite this article: Jie Sun *et al* 2020 *Nanotechnology* **31** 115701

View the [article online](#) for updates and enhancements.



**IOP | ebooks™**

Bringing together innovative digital publishing with leading authors from the global scientific community.

Start exploring the collection—download the first chapter of every title for free.

# Low thermal conductivity of peanut-shaped carbon nanotube and its insensitive response to uniaxial strain

Jie Sun<sup>1</sup>, Kunpeng Yuan<sup>2</sup>, Wenyang Zhou<sup>1</sup>, Xiaoliang Zhang<sup>2</sup>, Jun Onoe<sup>3</sup>, Y Kawazoe<sup>4,5</sup> and Qian Wang<sup>1</sup> 

<sup>1</sup> Center for Applied Physics and Technology, Department of Materials Science and Engineering, HEDPS, College of Engineering, Peking University, Beijing 100871, People's Republic of China

<sup>2</sup> Key Laboratory of Ocean Energy Utilization and Energy Conservation of Ministry of Education, School of Energy and Power Engineering, Dalian University of Technology, Dalian 116024, People's Republic of China

<sup>3</sup> Department of Energy Science and Engineering, Nagoya University, Nagoya, 4648603, Japan

<sup>4</sup> New Industry Creation Hatchery Center, Tohoku University, Sendai, 980-8577, Japan

<sup>5</sup> Suranaree University of Technology, Nakhon Ratchasima 30000, Thailand

Received 11 July 2019, revised 17 October 2019

Accepted for publication 25 November 2019

Published 23 December 2019



CrossMark

## Abstract

Motivated by the experimental synthesis of peanut-shaped carbon nanotubes (PSNTs) that combine the novel features of fullerene and carbon nanotubes (CNTs), we study the thermal conductivity of a PSNT (1dp08) and its response to different strains by using non-equilibrium molecular dynamics simulations and lattice dynamics together with density functional theory. We find that the thermal conductivity of the PSNT is reduced by more than 90% as compared to that of CNTs, and remains almost the same when different strains applied, exhibiting very different behaviors from that of CNTs, where the thermal conductivity decreases monotonically with the increase of strain. Through phonon mode calculations, we show that the reduced phonon group velocity, phonon lifetime and the vibrational mismatch are responsible for the low thermal conductivity of the PSNT, and the insensitive response of thermal conductivity to strain is due to the insensitivity of its phonon density of states and group velocity to strain. These features endow the PSNT with the potential applications in thermal devices, and add new features to one-dimensional carbon nanomaterials going beyond conventional CNTs.

Keywords: peanut-shaped carbon nanotubes, thermal conductivity, molecular dynamics, lattice dynamics

(Some figures may appear in colour only in the online journal)

## Introduction

Carbon allotropes have attracted a widespread attention in the last few decades. Due to the flexibility of its orbital hybridization, carbon can form various materials with their structures ranging from zero-dimension (0D) to three-dimension, exhibiting many fascinating properties, such as the extremely high Young's modulus of carbon nanotubes (CNTs) [1–3], the super-high carrier mobility in graphene [4–6], and the superhardness of diamond [7]. Among all these physical

properties, the thermal conductivity is of particular interest because it can change in a wide range from 0.01 to 5000 W mK<sup>-1</sup> or even higher [8]. For example, the thermal conductivity of fullerene nanofluid is 0.4 W mK<sup>-1</sup> at room temperature [9], while that of some CNTs can reach 6600 W mK<sup>-1</sup> [10]. Different from the high thermal conductivity of one-dimensional (1D) CNTs, another 1D carbon allotrope, named diamond nanothreads [11–13], exhibits low thermal conductivity of 55 W mK<sup>-1</sup> [14]. Such a huge difference in the thermal conductivity of these carbon allotropes

shows the possibility of tuning the thermal transport properties of carbon materials by changing dimensionality and morphology for different applications [15–19].

Fullerene  $C_{60}$  and its assembled thin films are well known carbon allotropes, from which other structures can be derived. For example, two fullerene  $C_{60}$  can form a peanut-shaped dimer proposed by Strout *et al* in 1993 [20], and synthesized by Onoe *et al* in 1999 [21], which has attracted a great deal of interest [22–31]. Further studies have shown that peanut-shaped dimers can be encapsulated in single-wall CNTs forming PSNTs [32, 33]. Later on Takashima *et al* [34], found that a PSNT can be formed with its structural unit of P08  $C_{120}$  isomer, called 1dp08, when pristine fullerene  $C_{60}$  films were irradiated by using electron beam with an incident intensity of 3 keV. PSNTs can be considered as a 1D assembly of fullerene  $C_{60}$  integrating the features of nanocage and nanotube, exhibiting the negative Gaussian curvature and the polarized charges [30]. These intriguing properties have stimulated many studies on PSNTs. For instance, the electronic and electron-transport properties and Peierls transition of PSNTs were studied by Onoe *et al* [35]. The electronic states of different PSNT models generated using Stone–Wales transformations were studied by Yusuke *et al* [31]. The application of a metallic PSNT in capturing  $CO_2$  was explored by Zhao *et al* [36]. However, no any studies on the thermal transport properties of PSNTs have been reported so far, which motivates us to carry out this study.

In this paper, we take one of these PSNTs, i.e. 1dp08 [34], as an example, to study its thermal conductivity and response to strain by using non-equilibrium molecular dynamics (NEMD) method combined with density functional theory (DFT). We further elucidate how the thermal conductivity of the PSNT is different from that of CNTs by choosing two CNTs with the chirality of (5, 5) and (9, 0), respectively, for comparison, because their diameters are close to that of the PSNT.

## Computational methods

We use NEMDs method as implemented in the large-scale atomic/molecular massively parallel simulation molecular dynamics package to do the simulations with Tersoff potential for carbon proposed by Lindsay and Broido in 2010 [37]. This potential can well describe the thermal conductivity of many carbon-based materials, such as CNTs and graphene [38–40]. To have a fair comparison, we choose this potential to calculate the thermal conductivities of CNTs and PSNTs. The temperature is controlled by adding/subtracting heat at the heat reservoir/sink. Fixed walls are set at both ends of the structures. The thermal conductivities are obtained by using Fourier law:  $\kappa = J/\nabla T$ , where  $\kappa$ ,  $J$  and  $\nabla T$  are the thermal conductivity, heat flux and temperature gradient, respectively. In calculating the thermal conductivity using LAMMSP code, the simulation time step is set to 0.5 femtosecond (fs) and a large vacuum space of 100 Å is included along the transverse directions. The structures are first relaxed in NPT ensemble for  $5 \times 10^6$  steps, pressure in the length direction is set to be

zero. Then, the structures are thermalized in NVT ensemble for  $5 \times 10^6$  steps at temperature of 300 K, and further thermalized in NVE ensemble for another  $5 \times 10^6$  steps until the system reaches its steady state. To get the steady temperature gradient, we first let the structures evolve for  $1.0 \times 10^6$  time steps, and then let them last for  $1.9 \times 10^7$  time steps.

For Young's modulus calculation, a large vacuum space of 100 Å is included along the transverse directions. The optimized Tersoff potential is used with a time step of 1 fs. Before the deformation simulation, the conjugate gradient method is used to do the energy minimization, and the structures are relaxed in NPT ensemble for 50 ps. The deformations along the axial direction are simulated at a strain rate of  $1 \times 10^8 \text{ s}^{-1}$  at 300 K in NVE ensemble.

Energy band structure is calculated based on first principles calculations within the framework of DFT. The projector augmented gradient wave method [41] implemented in the Vienna *Ab initio* Simulation Package [42, 43] with the generalized gradient approximation [44] for the exchange-correlation functional formulated by Perdew–Burke–Ernzerhof is used. The energy cutoff is set to 500 eV, and the convergence criteria of total energy and force components are set to 0.0001 eV and  $0.01 \text{ eV \AA}^{-1}$ , respectively. A vacuum space of 15 Å is set perpendicular to the axial direction. A  $11 \times 1 \times 1$  Monkhorst–Pack K point mesh is adopted [45].

Spectral energy density analysis (SED) is used to analyze the relative contribution of phonons with different frequencies to the thermal conductivity [46–49], where the phonon normal modes can be written as

$$Q(\mathbf{k}, \mu, t) = \sum_{jl} \sqrt{\frac{m_j}{N}} \mathbf{v}_{jl}(t) \cdot \mathbf{e}_j^*(\mathbf{k}, \mu) \exp(-2\pi i \mathbf{k} \cdot \mathbf{r}_l), \quad (1)$$

where  $\mathbf{k}$  is the wave vector,  $\mu$  represents the phonon branch,  $m_j$  is the mass of  $j$ th atom,  $N$  is the number of unit cells,  $\mathbf{v}_{jl}$  is the velocity of  $j$ th atom located inside the  $l$ th unit cell ( $\mathbf{r}_l$ ), and  $\mathbf{e}_j^*(\mathbf{k}, \mu)$  is the eigenvector of phonon mode.

SED can be obtained by using the following equation:

$$\phi(\mathbf{k}, \mu, f) = \left| \int Q(\mathbf{k}, \mu, t) \exp(-2\pi i f t) dt \right|^2. \quad (2)$$

In addition, the detailed expression of SED can be also written as

$$\phi(\mathbf{k}, \mu, f) = \frac{I}{1 + \left[ \frac{2\pi [f - f_0(\mathbf{k}, \mu)]}{\Gamma(\mathbf{k}, \mu)} \right]^2}, \quad (3)$$

where  $I$  is the peak magnitude,  $f_0(\mathbf{k}, \mu)$  is the frequency at the peak center, and  $\Gamma(\mathbf{k}, \mu)$  is the half width at half-maximum. Phonon lifetime can be obtained by fitting the function  $\tau(\mathbf{k}, \mu) = 1/2\Gamma(\mathbf{k}, \mu)$ .

The mode dependent thermal conductivity can be derived from phonon Boltzmann transport equation under the relaxation time approximation [50, 51]

$$k_\alpha = \sum_{\mathbf{k}} \sum_{\mu} c_{ph} v_{g,\alpha}^2(\mathbf{k}, \mu) \tau(\mathbf{k}, \mu), \quad (4)$$

where  $k_\alpha$ ,  $c_{ph}$ ,  $v_{g,\alpha}$  represent the thermal conductivity in the  $\alpha$

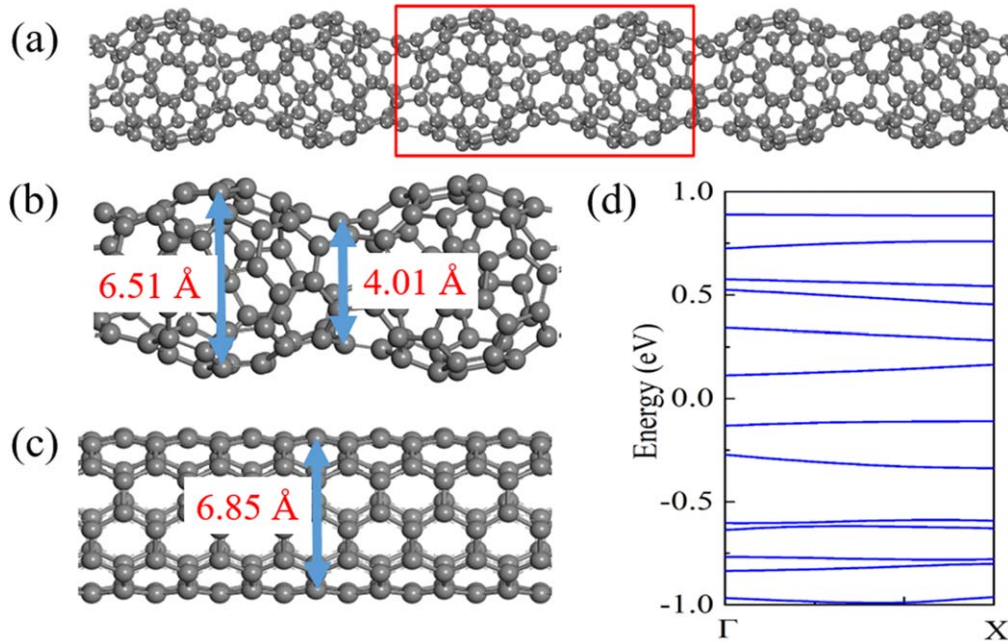


**Figure 1.** (a) Geometric structure of (a) the PSNT, 1dp08, (b) the structure unit of 1dp08, and (c) (5, 5) CNT. (d) Band structure of 1dp08.

direction, phonon volumetric specific heat, and phonon group velocity, respectively.  $c_{ph}$  can be calculated by using  $k_B/V$ , where  $k_B$  is Boltzmann constant, and  $V$  is system volume. By solving the dynamic matrices, we can get phonon dispersion curves. Group velocity can be calculated by  $\partial\omega/\partial k$ , where  $\omega$  and  $k$  denote eigenfrequency and wave vector, respectively.

## Results and discussion

### Geometry and band structure

The geometric structure of the PSNT, 1dp08, is plotted in figure 1(a). In NEMD simulations, the cross-sectional area is needed for calculating the heat flux. For the PSNT, the size of the cross sections is not equal to each other, as shown in figure 1(b). The average diameter is calculated to be 5.26 Å by using the maximum diameter (6.51 Å) and minimum diameter (4.01 Å). The physical diameter used in the calculations usually takes the value of the average diameter plus the van der Waals radius of two carbon atoms (3.40 Å). Therefore, the physical diameter of the PSNT is 8.66 Å. For comparison, calculations are also performed to (5, 5) and (9, 0) CNTs as their radial size is close to the average one of the PSNT. For (5, 5) CNT, the diameter is 6.58 Å, as shown in figure 1(c), while that of (9, 0) CNT is 7.10 Å. Therefore, the physical diameters for (5, 5) and (9, 0) CNTs used for our calculations are 9.98 and 10.50 Å, respectively.

We calculate the band structure of the PSNT. The unit cell contains 120 atoms and the results are plotted in figure 1(d). For the sake of clarity, we only plot the bands near the Fermi level with their energies in the range of  $-1.00$  eV to  $1.00$  eV. The valence band maximum is  $-0.11$  eV and the conduction band minimum (CBM) is  $0.10$  eV. One can see that the PSNT is a semiconductor with a band gap of  $0.21$  eV

and (9, 0) CNT also exhibits a band gap of  $0.07$  eV, consistent with previous studies [52, 53]. Usually, in semiconductors, the lattice vibration makes dominant contribution to their heat transport. While (5, 5) CNT is metallic.

### Thermal conductivity

To study the thermal conductivity of the PSNT and CNTs with different lengths at room temperature, we first calculate the temperature distributions along the heat flux direction of the PSNT and CNTs with the length of 50 nm. The results are plotted in figure 2(a), which shows that the temperature distribution has a linear relationship between the hot and cold ends, implying that the parameters that we set in the MD simulation is appropriate as the stable and linear temperature distribution is obtained. The nonlinear part at the hot and cold ends is caused by the edge effects, suggesting that the thermal transport is not fully diffusive. In order to avoid the edge effects, only the linear part is taken to calculate the temperature gradient. Following the same procedure, we also carry out the calculations for (5, 5) and (9, 0) CNTs, and plot the results in figure 2(a).

We then calculate the thermal conductivity. Usually, in NEMD simulation, finite-size effect happens when the size of a model is shorter than its phonon mean-free path [54, 55], consequently, its thermal conductivity is affected. Scattering occurring at the interfaces of the heat and cold ends account for such phenomenon. The thermal conductivity of the PSNT with length of 50, 100, 300, 500, 800 and 1000 nm is calculated to be 18.64, 23.96, 65.98, 75.98, 94.12 and 93.75  $\text{W mK}^{-1}$ , respectively, as seen in figure 2(b). The results show that the thermal conductivity of PSNT has reached a plateau of  $94 \text{ W mK}^{-1}$  with the length of 800 nm. For (5, 5) CNT, the thermal conductivities for the corresponding lengths are calculated to be 305.88, 457.14, 684.22,

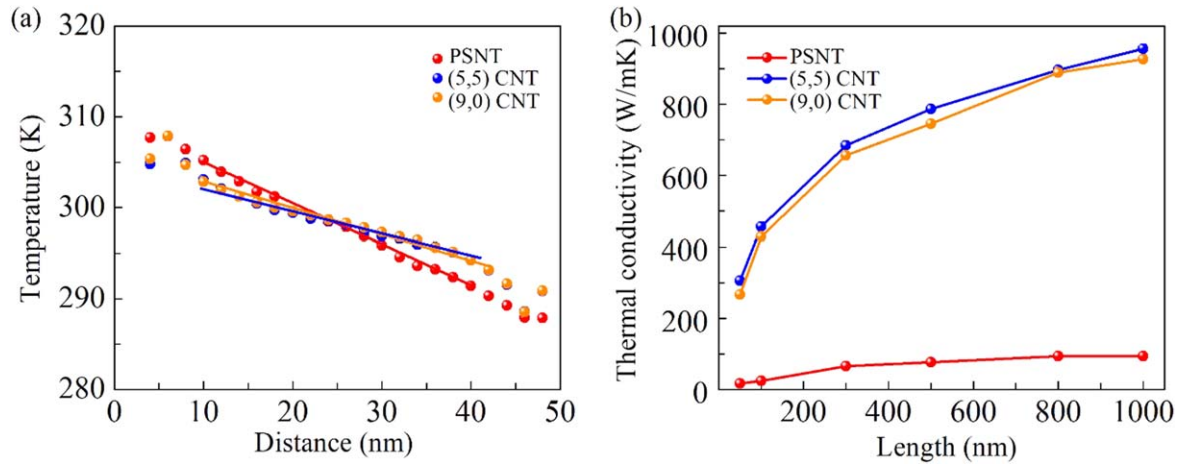


**Figure 2.** (a) Temperature profile, and (b) variation of the thermal conductivity with the size (length) for the PSNT, and (5, 5) and (9, 0) CNTs, respectively.

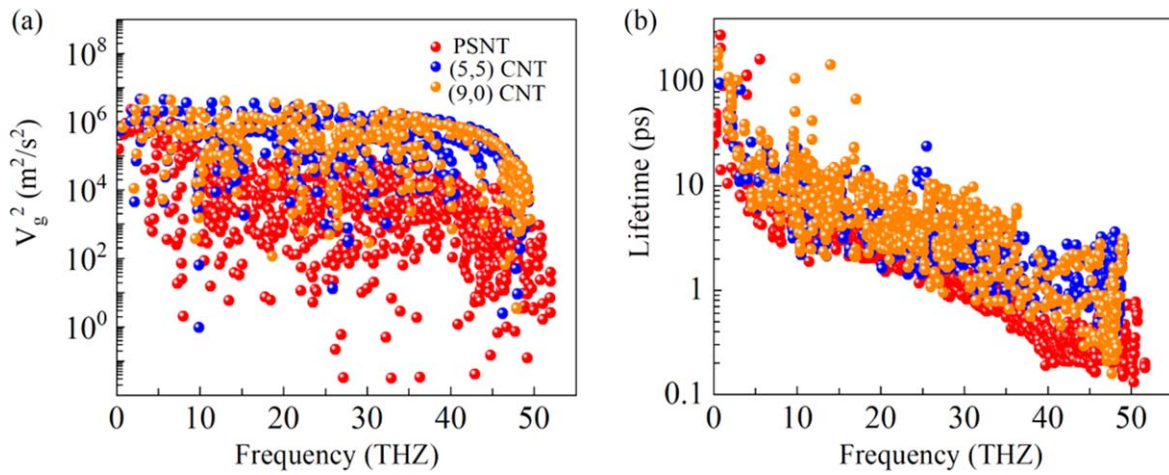


**Figure 3.** (a) Square group velocity, and (b) phonon lifetime versus frequency for the PSNT, (5, 5) and (9, 0) CNTs.

786.68, 896.55 and 956.52  $W mK^{-1}$ , respectively. While for (9, 0) CNT, the corresponding values are 266.67, 428.62, 656.25, 745.72, 888.89 and 926.72  $W mK^{-1}$ , respectively. The results for CNTs are consistent with previous studies [56]. One can see that although the thermal conductivity for all the three systems increases with increasing the length due to the finite-size effect, that of the PSNT is much smaller than the corresponding values of CNTs. For instance, for the systems with length of 500 nm, the thermal conductivity of the PSNT is 75.98  $W mK^{-1}$ , which is only about one tenth of that of the CNTs.

It is interesting to note such a huge decrease in the thermal conductivity of PSNT compared with that of CNTs. This can be partially attributed to the fact that PSNT has negative curvature that can reduce the thermal conductivity by several orders of magnitude as found in other carbon structures [57]. In order to explore the reasons why the PSNT has such low thermal conductivity, as compared to the CNTs, we study the phonon properties. We first calculate the squared phonon group velocity and phonon lifetime for the PSNT, and the CNTs as well. The results are plotted in figures 3(a) and (b), respectively. Figure 3(a) shows that the square group

velocities of the PSNT are much lower than those of the CNTs in the region from 10 to 50 THz, and most of the values are lower than  $2000 m^2 s^{-2}$ . While almost half of the values of the CNTs are higher than  $5000 m^2 s^{-2}$ . Figure 3(b) shows that the phonon lifetime of the PSNT is also much lower than that of the CNTs in most of the frequency region from 0 to 50 THz. For instance, the average phonon lifetime for the PSNT in low frequency region (0–5 THz), middle frequency region (5–30 THz) and high frequency region (30–50 THz) is 39.49, 3.11 and 0.96 picoseconds (ps), respectively. For (5, 5) CNT, the corresponding value is 51.61, 7.89 and 2.18 ps and for (9, 0) CNT, the corresponding value is 42.68, 8.08 and 4.56 ps, respectively. From the average lifetime in the different regions, one can see that the phonons with low and middle frequencies contribute more to the difference in thermal conductivity between the PSNT and CNTs. Especially in middle regions, the average phonon lifetime of the CNTs is about twice larger than that of the PSNT.

We next calculate the vibrational density of states (VDOS), which describes the frequency distribution of phonons by taking a Fourier transform on the atom velocity autocorrelation function [58, 59]. We choose two different

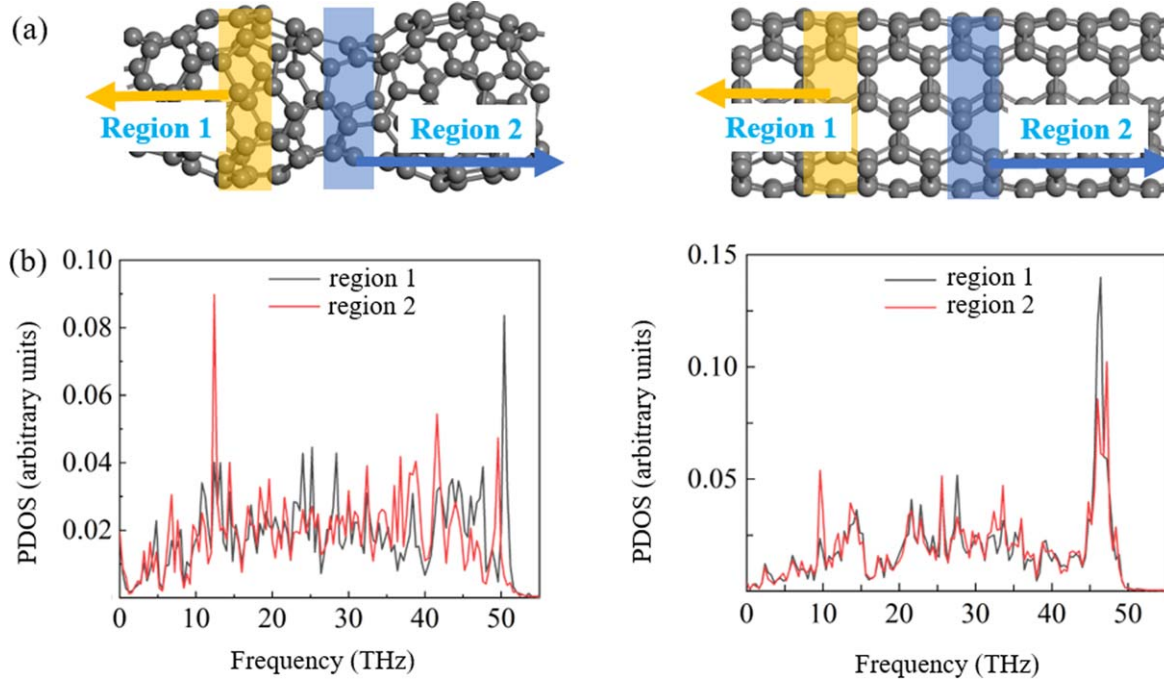


**Figure 4.** (a) Schematic diagrams of the two regions, and (b) VDOS for the PSNT and (9, 0) CNT.

regions for the PSNT and (9, 0) CNT, as shown in figure 4(a), to calculate their VDOS. The calculated results are plotted in figure 4(b). It is obvious that the VDOS of PSNT in the two regions are different from each other, especially, the peak of VDOS for region 1 has a right shift comparing to that of region 2 in the frequency range of 45–50 THz. However, the VDOS of the CNT in the two regions is nearly overlapped. We use the phonon population variation ratio to reflect the VDOS overlap by using the following equation [60, 61]:

$$\Delta n(\omega) = \frac{1 + \int_0^\omega \text{VDOS}_{\text{region1}}(\omega') d\omega'}{1 + \int_0^\omega \text{VDOS}_{\text{region2}}(\omega') d\omega'}, \quad (5)$$

where  $\text{VDOS}_{\text{region1}}(\omega')$  and  $\text{VDOS}_{\text{region2}}(\omega')$  represent VDOS of region 1 and region 2 in the structures. According to equation (5), the phonon population variation ratios of the two regions for the PSNT and (9, 0) CNT are calculated to be 0.04% and 0.01%, respectively, showing that the overlap of VDOS in the PSNT is less than that in the CNT, due to the more vibrational mismatch in the PSNT. Therefore, the heat transfer efficiency would be hindered more in the PSNT than that in the CNT because of the larger vibrational mismatch when heat flux travels across the two regions, thus resulting in the low thermal conductivity of the PSNT. Such phenomenon was also observed in other study [59].

We then calculate the Young's moduli to further understand the mechanism of the low thermal conductivity. Young's modulus is associated with the stiffness of atomic bonds in a material. Weaker interatomic bonding usually leads to smaller stiffness and Young's modulus. For materials with low Young's modulus, their interatomic bonding is often seen as 'soft bonding', which can result in low transport velocities of phonons, thus leading to a lower lattice thermal

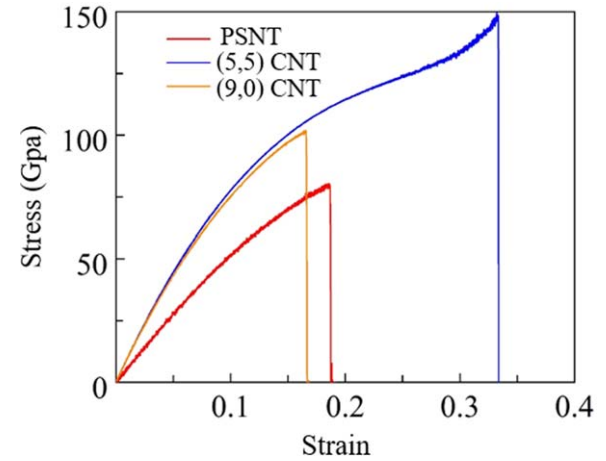


**Figure 5.** Stress–strain curves of PSNT, (5, 5) CNT and (9, 0) CNT.

conductivity [62–65]. The stress–strain curves are shown in figure 5. The Young's moduli of the PSNT, (5, 5) and (9, 0) CNTs are calculated to be 0.56, 0.89 and 0.86 TPa, respectively, and the stress and strain remain linear relationship when strain is less than 10%. Note that the calculated Young's moduli for the CNTs are consistent with the previous results [66]. The smaller Young's modulus of the PSNT is one of the reasons accounting for the low thermal conductivity as compared with that of CNTs.

#### Strain-dependence of thermal conductivity

In practical applications, PSNTs cannot be in free state, and stress may exist due to the interactions with other parts in device. To see how sensitive of the thermal conductivity of the PSNT to strain, we study the thermal conductivity of the

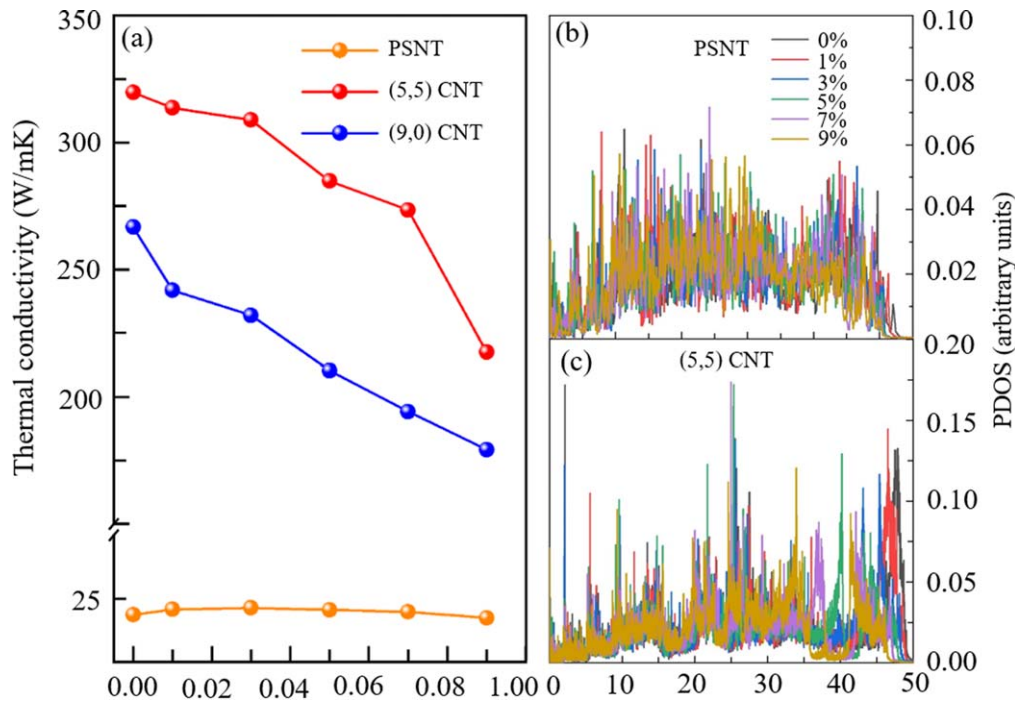


**Figure 6.** Thermal conductivity of (a) the PSNT, (5, 5) and (9, 0) CNT with the length of 50 nm versus strain. PDOS of (b) the PSNT and (c) (5, 5) CNT versus the frequency under different strains.

PSNT and CNTs when they are under uniaxial strains. We choose the length of 50 nm as an example to do the simulation. The strains are set as 1%, 3%, 5%, 7%, and 9%, their corresponding thermal conductivities of the PSNT are calculated to be 20.78, 21.40, 20.60, 19.78, and 17.40 W mK<sup>-1</sup>, respectively. Under strains, the thermal conductivities of (5, 5) CNT are 313.62, 308.92, 284.88 and 273.40 W mK<sup>-1</sup>, and corresponding values for (9, 0) CNT are 241.81, 231.91, 210.37 and 179.22 W mK<sup>-1</sup>, respectively. Obviously, very different from that of the CNTs, the thermal conductivity of the PSNT remains almost the same when under the different strains, insensitive to strain. For both (5, 5) and (9, 0) CNTs, the thermal conductivities decrease monotonously as strain increases. For clarity, these results are shown in figure 6(a).

To understand the reasons why the PSNT and CNTs have different responses to strain, we first calculate the phonon density of states (DOS) for the PSNT, and (5, 5) CNT for comparison. The calculated results are plotted in figure 6(b) and (c), which show that the phonon redshift is unobvious for PSNT, different from the situation in the CNT. We then calculate the phonon dispersion for the two systems. For clarity, we only plot the results of phonon dispersion under strains of 0%, 5% and 9%, respectively in figure 7. For the PSNT, both the acoustic and optical branches do not have a decline trend in slope, suggesting that the phonon group velocity of the PSNT under different strains remains almost unchanged, leading to the similar thermal conductivities. The phonon dispersion curves of the CNT without any strain are highly dispersive for acoustic and optical branches, which is consistent with previous study [67]. The frequencies of optical branches decrease gradually when strain is applied, leading to the decrease of phonon group velocity, thus

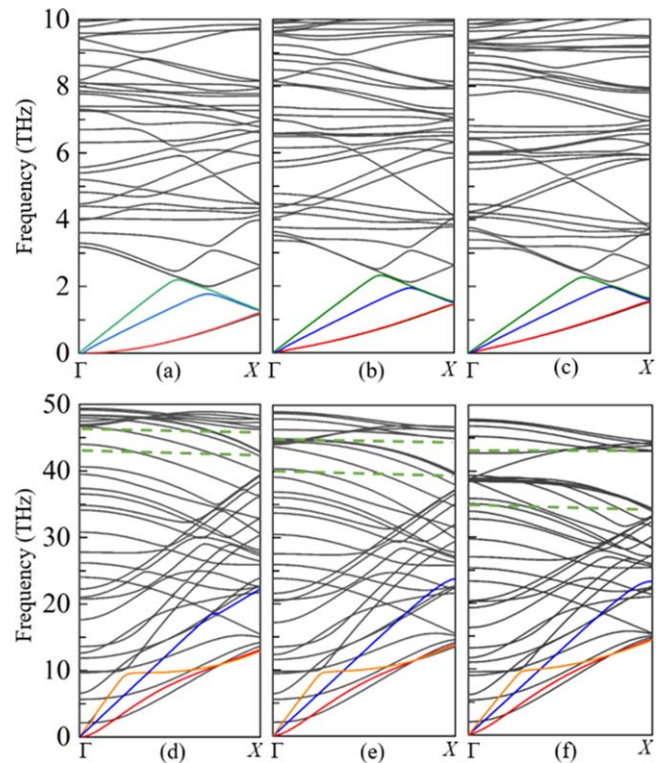


**Figure 7.** (a)–(c) Phonon dispersion of the PSNT under strain of 0.0%, 5% and 9%, respectively. (d)–(f) Phonon dispersion of (5, 5) CNT under strain of 0.0%, 5% and 9%, respectively.

accordingly reducing its thermal conductivity. The change in acoustic branches is not significant.

We next calculate the phonon velocities of the PSNT and CNT under different strains. The results are plotted in

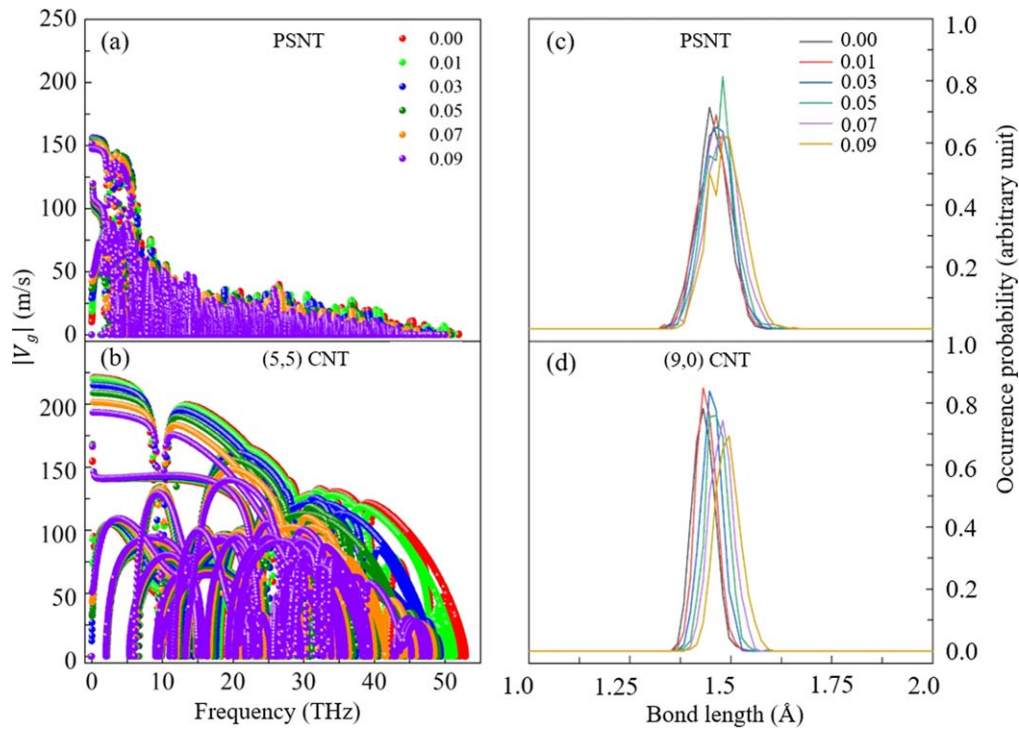


**Figure 8.** (a) and (b) Absolute values of phonon group velocities, and (c) and (d) occurrence probabilities under the different strains for the PSNT and CNT, respectively.

figure 8. Figure 8(a) shows that the phonon group velocities of the PSNT under different strains are almost the same in the entire frequency region, leading to the insensitive response of the thermal conductivity to the strain. While from figure 8(b), one can see that the absolute value of phonon group velocities of the (5, 5) CNT decreases with the increase of strain. In the low frequency region (0–10 THz), the group velocities under strains of 0.0%, 1%, 3% and 5% are larger than  $200 \text{ m s}^{-1}$ , while for the larger strains of 7% and 9%, the group velocities become lower than  $200 \text{ m s}^{-1}$ . The phonon group velocity decreases as the strain increases. In the low frequency region, some phonon group velocities decrease as the strain increases, while the others exhibit opposite characteristic. This explains why the phonon branches do not have an obvious decline in their corresponding slopes. As shown in figure 6(a), the thermal conductivity decreases slightly when strain is below 3%, while the thermal conductivity decreases more sharply when strain is above 5%. One can see that the group velocities of (5, 5) CNT under strains of 0.0% and 1% are close to each other. While, the difference becomes larger when strain is above 5%, which is consistent with the trend of thermal conductivity.

The response of thermal conductivity to strain can also be understood from the change of bond length. Previous studies showed that the thermal conductivity of CNT decreases with the increase of bond length induced by the applied tensile strain [68]. The deformation of a covalent bond includes the changes in bond length and bond angle. Here, we choose the bond length change for analysis. The bond length occurrence

probabilities of the PSNT and (9, 0) CNT under different strains are plotted in figures 8(c) and (d), respectively, which show that the bond-length change to strain for the PSNT is less sensitive than that of (9, 0) CNT. The insensitivity of the bond-length change to strain in the PSNT is also one of the reasons that lead to the insensitivity of thermal conductivity to strain.

We further calculate the potential energies of the PSNT and (9, 0) CNT to examine their response to strain because the potential energy of a material is also related to its thermal conductivity. Figure 9 shows the relative variance ratio of potential energy for the PSNT and (9, 0) CNT versus strain. The variance ratio is defined as  $E_s/E_0$ , where  $E_s$  and  $E_0$  are the total energies of a structure with and without strain, respectively. It is obvious that the potential energy of the PSNT is less sensitive to strain as compared to that of the CNT, indicating that the PSNT is less flexible for deformation. The flexibility can indirectly depict the degree of sensitivity of the thermal conductivity to strain.

## Conclusions

In this work, the thermal conductivity of a PSNT (1dp08) and its response to strain are studied for the first time by using molecular dynamics simulations combined with lattice dynamics and DFT. The thermal conductivities of the PSNTs with the length of 50, 100, 200, 300, and 500 nm are calculated to be 18.64, 23.96, 65.98 and  $75.98 \text{ W mK}^{-1}$ ,

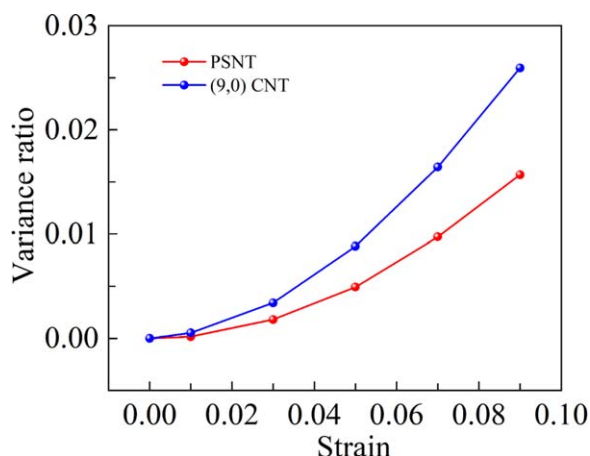


**Figure 9.** Variance ratio of the potential energies of the PSNT and (9, 0) CNT versus strain.

respectively, which are only about one tenth of those of the corresponding CNTs. A detailed phonon mode analysis reveals that the main reasons of the low thermal conductivity of the PSNT are the reduced phonon group velocity, reduced phonon lifetime and more vibrational mismatch, as compared with those of the CNTs. In addition, we have shown that the small Young's modulus, and the insensitive bond-length change and potential energy to strain of PSNT account for the insensitive response of its thermal conductivity to strain. These findings suggest that the unusual thermal transport properties of PSNT is induced by its unique geometry of peanut-shape distinguishing from that of CNTs. The low thermal conductivity of the PSNT and its insensitivity to strain add new features to 1D carbon family going beyond the conventional CNTs. This study provides an insightful understanding of the thermal transport properties of PSNTs that integrate the feature of cage and tube for potential technological applications.

## Acknowledgments

This work is partially supported by grants from the National Key Research and Development Program of the Ministry of Science and Technology of China (Grant Nos. 2016YFE0127300 and 2017YFA 0205003), the National Natural Science Foundation of China (Grant Nos. 11974028 and 21773004), and is supported by the High Performance Computing Platform of Peking University, China. The authors thank the crew of the Center for Computational Materials Science, the Institute for Materials Research, Tohoku University (Japan), for their continuous support of the Hitachi SR16000 supercomputing facility. Y K is thankful to the support by AOARD for the grant of FA2386-18-1-4050.

## ORCID iDs

Qian Wang  <https://orcid.org/0000-0002-9766-4617>

## References

- [1] Salvétat J-P, Bonard J-M, Thomson N, Kulik A, Forro L, Benoit W and Zuppiroli L 1999 Mechanical properties of carbon nanotubes *Appl. Phys.* **69** 255–60
- [2] Yu M-F, Files B S, Arepalli S and Ruoff R S 2000 Tensile loading of ropes of single wall carbon nanotubes and their mechanical properties *Phys. Rev. Lett.* **84** 5552
- [3] Ruoff R S, Qian D and Liu W K 2003 Mechanical properties of carbon nanotubes: theoretical predictions and experimental measurements *C.R. Phys.* **4** 993–1008
- [4] Bolotin K I, Sikes K, Jiang Z, Klima M, Fudenberg G, Hone J, Kim P and Stormer H 2008 Ultrahigh electron mobility in suspended graphene *Solid State Commun.* **146** 351–5
- [5] Hwang E and Sarma S D 2008 Acoustic phonon scattering limited carrier mobility in two-dimensional extrinsic graphene *Phys. Rev.* **77** 115449
- [6] Ponomarenko L, Yang R, Mohiuddin T, Katsnelson M, Novoselov K, Morozov S, Zhukov A, Schedin F, Hill E and Geim A 2009 Effect of a high- $\kappa$  environment on charge carrier mobility in graphene *Phys. Rev. Lett.* **102** 206603
- [7] Li Z, Gao F and Xu Z 2012 Strength, hardness, and lattice vibrations of Z-carbon and W-carbon: first-principles calculations *Phys. Rev.* **85** 144115
- [8] Balandin A A 2011 Thermal properties of graphene and nanostructured carbon materials *Nat. Mater.* **10** 569
- [9] Y-j H, Lee J, Lee C, Jung Y, Cheong S, Lee C, Ku B and Jang S 2007 Stability and thermal conductivity characteristics of nanofluids *Thermochim. Acta* **455** 70–4
- [10] Berber S, Kwon Y-K and Tománek D 2000 Unusually high thermal conductivity of carbon nanotubes *Phys. Rev. Lett.* **84** 4613
- [11] Fitzgibbons T C, Guthrie M, Xu E-S, Crespi V H, Davidowski S K, Cody G D, Alem N and Badding J V 2015 Benzene-derived carbon nanotubes *Nat. Mater.* **14** 43
- [12] Zhan H, Zhang G, Tan V B and Gu Y 2017 The best features of diamond nanothread for nanofibre applications *Nat. Commun.* **8** 14863
- [13] Juhl S J, Wang T, Vermilyea B, Li X, Crespi V H, Badding J V and Alem N 2019 Local structure and bonding of carbon nanotubes probed by high-resolution transmission electron microscopy *J. Am. Chem. Soc.* **141** 6937–45
- [14] Zhan H, Zhang G, Zhang Y, Tan V, Bell J M and Gu Y 2016 Thermal conductivity of a new carbon nanotube analog: the diamond nanothread *Carbon* **98** 232–7
- [15] Blackburn J L, Ferguson A J, Cho C and Grunlan J C 2018 Carbon-nanotube-based thermoelectric materials and devices *Adv. Mater.* **30** 35
- [16] Amiri A, Shanbedi M, Chew B T, Kazi S N and Solangi K H 2016 Toward improved engine performance with crumpled nitrogen-doped graphene based water-ethylene glycol coolant *Chem. Eng. J.* **289** 583–95
- [17] Lin Y X, Jia Y T, Alva G and Fang G Y 2018 Review on thermal conductivity enhancement, thermal properties and applications of phase change materials in thermal energy storage *Renew. Sust. Energy Rev.* **82** 2730–42
- [18] Pang Z, Gu X, Wei Y, Yang R and Dresselhaus M S 2017 Bottom-up design of three-dimensional carbon-honeycomb with superb specific strength and high thermal conductivity *Nano Lett.* **17** 179–85
- [19] Kholmanov I, Kim J, Ou E, Ruoff R S and Shi L 2015 Continuous carbon nanotube-ultrathin graphite hybrid foams for increased thermal conductivity and suppressed subcooling in composite phase change materials *ACS Nano* **9** 11699–707
- [20] Strout D L, Murry R L, Xu C, Eckhoff W C, Odom G K and Scuseria G E 1993 A theoretical study of

- buckminsterfullerene reaction products: C<sub>60</sub> + C<sub>60</sub> *Chem. Phys. Lett.* **214** 576–82
- [21] Onoe J, Hashi Y-i, Esfarjani K, Hara T, Kawazoe Y and Takeuchi K 1999 In-situ infrared spectroscopy of a photoirradiated potassium-doped C<sub>60</sub> film *Chem. Phys. Lett.* **315** 19–24
- [22] Hara T and Onoe J 2003 Vibrational analysis of peanut-shaped C<sub>120</sub> fullerenes *Eur. Phys. J. D* **24** 389–92
- [23] Wang G, Li Y and Huang Y 2005 Structures and electronic properties of peanut-shaped dimers and carbon nanotubes *J. Phys. Chem.* **109** 10957–61
- [24] Onoe J, Nakayama T, Aono M and Hara T 2003 Structural and electrical properties of an electron-beam-irradiated C<sub>60</sub> film *Appl. Phys. Lett.* **82** 595–7
- [25] Beu T A, Onoe J and Hida A 2005 First-principles calculations of the electronic structure of one-dimensional C<sub>60</sub> polymers *Phys. Rev.* **72** 155416
- [26] Nakayama H, Ono T, Goto H and Hirose K 2007 Electronic structures of peanut-shaped fullerene tubes *Sci. Technol. Adv. Mater.* **8** 196
- [27] Onoe J, Nakayama T, Aono M and Hara T 2004 The electron transport properties of photo- and electron-beam-irradiated C<sub>60</sub> films *J. Phys. Chem. Solids* **65** 343–8
- [28] Ono S and Shima H 2011 Phonon dispersion and electron-phonon interaction in peanut-shaped fullerene polymers *J. Phys. Soc. Jpn.* **80** 064704
- [29] Noda Y and Ohno K 2011 Metallic and non-metallic properties of one-dimensional peanut-shaped fullerene polymers *Synth. Met.* **161** 1546–51
- [30] Onoe J, Ito T, Shima H, Yoshioka H and Kimura S-I 2012 Observation of riemannian geometric effects on electronic states *Europhys. Lett.* **98** 27001
- [31] Noda Y, Ono S and Ohno K 2015 Geometry dependence of electronic and energetic properties of one-dimensional peanut-shaped fullerene polymers *J. Phys. Chem.* **119** 3048–55
- [32] Bandow S, Takizawa M, Hirahara K, Yudasaka M and Iijima S 2001 Raman scattering study of double-wall carbon nanotubes derived from the chains of fullerenes in single-wall carbon nanotubes *Chem. Phys. Lett.* **337** 48–54
- [33] Sloan J, Dunin-Borkowski R E, Hutchison J L, Coleman K S, Williams V C, Claridge J B, York A P, Xu C, Bailey S R and Brown G 2000 The size distribution, imaging and obstructing properties of C<sub>60</sub> and higher fullerenes formed within arc-grown single walled carbon nanotubes *Chem. Phys. Lett.* **316** 191–8
- [34] Takashima A, Nishii T and Onoe J 2012 Formation process and electron-beam incident energy dependence of one-dimensional uneven peanut-shaped C<sub>60</sub> polymer studied using *in situ* high-resolution infrared spectroscopy and density-functional calculations *J. Phys. D: Appl. Phys.* **45** 485302
- [35] Onoe J, Ochiai Y, Ito T, Kimura S, Ueda S, Noguchi Y and Ohno K 2007 Electronic and electron-transport properties of peanut-shaped C<sub>60</sub> polymers *J. Phys. Conf. Series* **61** 899–903
- [36] Zhao T, Wang Q, Kawazoe Y and Jena P 2018 A metallic peanut-shaped carbon nanotube and its potential for CO<sub>2</sub> capture *Carbon* **132** 249–56
- [37] Lindsay L and Broido D 2010 Optimized tersoff and brenner empirical potential parameters for lattice dynamics and phonon thermal transport in carbon nanotubes and graphene *Phys. Rev.* **81** 205441
- [38] Bagri A, Kim S-P, Ruoff R S and Shenoy V B 2011 Thermal transport across twin grain boundaries in polycrystalline graphene from nonequilibrium molecular dynamics simulations *Nano Lett.* **11** 3917–21
- [39] Salaway R N and Zhigilei L V 2014 Molecular dynamics simulations of thermal conductivity of carbon nanotubes: Resolving the effects of computational parameters *Int. J. Heat Mass Transfer* **70** 954–64
- [40] Säskilähti K, Oksanen J, Volz S and Tulkki J 2015 Frequency-dependent phonon mean free path in carbon nanotubes from nonequilibrium molecular dynamics *Phys. Rev.* **91** 115426
- [41] Blöchl P E 1994 Projector augmented-wave method *Phys. Rev.* **50** 17953–79
- [42] Kresse G and Furthmüller J 1996 Efficient iterative schemes for *ab initio* total-energy calculations using a plane-wave basis set *Phys. Rev.* **54** 11169–86
- [43] Kresse G and Furthmüller J 1996 Efficiency of *ab-initio* total energy calculations for metals and semiconductors using a plane-wave basis set *Comput. Mater. Sci.* **6** 15–50
- [44] Perdew J P, Burke K and Ernzerhof M 1996 Generalized gradient approximation made simple *Phys. Rev. Lett.* **77** 3865–8
- [45] Monkhorst H J and Pack J D 1976 Special points for Brillouin-zone integrations *Phys. Rev.* **13** 5188
- [46] Larkin J, Turney J, Massicotte A, Amon C and McGaughey A 2014 Comparison and evaluation of spectral energy methods for predicting phonon properties *J. Comput. Theor. Nanosci.* **11** 249–56
- [47] Zhou Y, Zhang X and Hu M 2015 Quantitatively analyzing phonon spectral contribution of thermal conductivity based on nonequilibrium molecular dynamics simulations: I. From space Fourier transform *Phys. Rev.* **92** 195204
- [48] Zhang X, Bao H and Hu M 2015 Bilateral substrate effect on the thermal conductivity of two-dimensional silicon *Nanoscale* **7** 6014–22
- [49] Gao Y, Zhang X, Zhou Y and Hu M 2017 Giant reduction in thermal conductivity of extended type-I silicon clathrates and prominent thermal effect of 6d guest Wyckoff positions *J. Mater. Chem.* **5** 10578–88
- [50] Zhang X, Gao Y, Chen Y and Hu M 2016 Robustly engineering thermal conductivity of bilayer graphene by interlayer bonding *Sci. Rep.* **6** 22011
- [51] Ladd A J, Moran B and Hoover W G 1986 Lattice thermal conductivity: a comparison of molecular dynamics and anharmonic lattice dynamics *Phys. Rev. B* **34** 5058
- [52] Cioslowski J, Rao N and Moncrieff D 2002 Electronic structures and energetics of 5, 5 and 9, 0 single-walled carbon nanotubes *J. Am. Chem. Soc.* **124** 8485–9
- [53] Laird E A, Kuemmeth F, Steele G A, Grove-Rasmussen K, Nygard J, Flensberg K and Kouwenhoven L P 2015 Quantum transport in carbon nanotubes *Rev. Mod. Phys.* **87** 703–64
- [54] Oligschleger C and Schön J 1999 Simulation of thermal conductivity and heat transport in solids *Phys. Rev.* **59** 4125
- [55] Poetzsch R H and Böttger H 1994 Interplay of disorder and anharmonicity in heat conduction: molecular-dynamics study *Phys. Rev.* **50** 15757
- [56] Alaghemandi M, Algaer E, Böhm M C and Müller-Plathe F 2009 The thermal conductivity and thermal rectification of carbon nanotubes studied using reverse non-equilibrium molecular dynamics simulations *Nanotechnology* **20** 115704
- [57] Zhang Z, Chen J and Li B 2017 Negative gaussian curvature induces significant suppression of thermal conduction in carbon crystals *Nanoscale* **9** 14208–14
- [58] Ren C, Zhang W, Xu Z, Zhu Z and Huai P 2010 Thermal conductivity of single-walled carbon nanotubes under axial stress *J. Phys. Chem.* **114** 5786–91
- [59] Hu M, Jing Y and Zhang X 2015 Low thermal conductivity of graphyne nanotubes from molecular dynamics study *Phys. Rev.* **91** 155408
- [60] Pereira L F C and Donadio D 2013 Divergence of the thermal conductivity in uniaxially strained graphene *Phys. Rev.* **87** 6
- [61] Zhan H F, Zhang G, Yang C H and Gu Y T 2018 Graphene helicoid: distinct properties promote application of graphene

- related materials in thermal management *J. Phys. Chem.* **122** 7605–12
- [62] Kurosaki K, Kosuga A, Muta H, Uno M and Yamanaka S 2005 Ag<sub>9</sub>TlTe<sub>5</sub>: a high-performance thermoelectric bulk material with extremely low thermal conductivity *Appl. Phys. Lett.* **87** 061919
- [63] Chiritescu C, Cahill D G, Nguyen N, Johnson D, Bodapati A, Keblinski P and Zschack P 2007 Ultralow thermal conductivity in disordered, layered WSe<sub>2</sub> crystals *Science* **315** 351–3
- [64] Li F, Li J-F, Zhao L-D, Xiang K, Liu Y, Zhang B-P, Lin Y-H, Nan C-W and Zhu H-M 2012 Polycrystalline BiCuSeO oxide as a potential thermoelectric material *Energy Environ. Sci.* **5** 7188–95
- [65] Pei Y L, He J Q, Li J F, Li F, Liu Q J, Pan W, Barreateau C, Berardan D, Dragoe N and Zhao L D 2013 High thermoelectric performance of oxyselenides: intrinsically low thermal conductivity of Ca-doped BiCuSeO *NPG Asia Mater.* **5** 9
- [66] Kok Z and Wong C H 2016 Molecular dynamics simulation studies of mechanical properties of different carbon nanotube systems *Mol. Simul.* **42** 1274–80
- [67] Zhang X, Hu M and Poulidakos D 2012 A low-frequency wave motion mechanism enables efficient energy transport in carbon nanotubes at high heat fluxes *Nano Lett.* **12** 3410–6
- [68] Wei N, Xu L, Wang H-Q and Zheng J-C 2011 Strain engineering of thermal conductivity in graphene sheets and nanoribbons: a demonstration of magic flexibility *Nanotechnology* **22** 105705